Published in final edited form as:
Histochem Cell Biol. 2010 March ; 133(3): 261–272. doi:10.1007/s00418-009-0672-3.

Characterization of endocytic compartments after holo-high density lipoprotein particle uptake in HepG2 cells

Clemens Röhrl,
Center for Physiology and Pathophysiology, Institute of Medical Chemistry, Medical University of Vienna, Vienna, Austria

Tamara A. Pagler,
Center for Physiology and Pathophysiology, Institute of Medical Chemistry, Medical University of Vienna, Vienna, Austria

Witta Strobl,
Center for Physiology and Pathophysiology, Institute of Medical Chemistry, Medical University of Vienna, Vienna, Austria

Adolf Ellinger,
Center for Anatomy and Cell Biology, Department of Cell Biology and Ultrastructure Research, Medical University of Vienna, Schwarzspanierstrasse 17, 1090 Vienna, Austria

Josef Neumüller,
Center for Anatomy and Cell Biology, Department of Cell Biology and Ultrastructure Research, Medical University of Vienna, Schwarzspanierstrasse 17, 1090 Vienna, Austria

Margit Pavelka,
Center for Anatomy and Cell Biology, Department of Cell Biology and Ultrastructure Research, Medical University of Vienna, Schwarzspanierstrasse 17, 1090 Vienna, Austria

Herbert Stangl, and
Center for Physiology and Pathophysiology, Institute of Medical Chemistry, Medical University of Vienna, Vienna, Austria

Claudia Meisslitzer-Ruppitsch
Center for Anatomy and Cell Biology, Department of Cell Biology and Ultrastructure Research, Medical University of Vienna, Schwarzspanierstrasse 17, 1090 Vienna, Austria

Abstract

Holo-high density lipoprotein (HDL) particle uptake, besides selective lipid uptake, constitutes an alternative pathway to regulate cellular cholesterol homeostasis. In the current study, the cellular path of holo-HDL particles was investigated in human liver carcinoma cells (HepG2) using combined light and electron microscopical methods. The apolipoprotein moiety of HDL was visualized with different markers: horseradish peroxidase, colloidal gold and the fluorochrome Alexa^{568}, used in fluorescence microscopy and after photooxidation correlatively at the ultrastructural level. Time course experiments showed a rapid uptake of holo-HDL particles, an accumulation in endosomal compartments, with a plateau after 1–2 h of continuous uptake, and a clearance 1–2 h upon replacement by unlabeled HDL. Correlative microscopy, using HDL-

Correspondence to: Claudia Meisslitzer-Ruppitsch.
claudia.meisslitzer-ruppitsch@meduniwien.ac.at.
Present Address: T. A. Pagler, Division of Molecular Medicine, Columbia University, New York, NY, USA

Europe PMC Funders Author Manuscripts

Alexa^{568}-driven diaminobenzidine (DAB) photooxidation, identified the fluorescent organelles as DAB-positive multivesicular bodies (MVBs) in the electron microscope; their luminal contents but not the internal vesicles were stained. Labeled MVBs increased in numbers and changed shapes along with the duration of uptake, from polymorphic organelles with multiple surface domains and differently shaped protrusions dominating at early times of uptake to compact bodies with mainly tubular appendices and densely packed vesicles after later times. Differently shaped and labeled surface domains and appendices, as revealed by three dimensional reconstructions, as well as images of homotypic fusions indicate the dynamics of the HDL-positive MVBs. Double staining visualized by confocal microscopy, along with the electron microscopic data, shows that holo-HDL particles after temporal storage in MVBs are only to a minor degree transported to lysosomes, which suggests that different mechanisms are involved in cellular HDL clearance, including resecretion.

Keywords

High density lipoprotein (HDL); Holo particle uptake; Correlative microscopy; Diaminobenzidine (DAB)-photooxidation; Electron tomography; Multivesicular bodies

Introduction

High density lipoprotein (HDL) exerts its anti-atherogenic effects by accepting cholesterol from peripheral cells (e.g., smooth muscle cell and macrophages) and transporting it to the liver for disposal, which altogether is termed reverse cholesterol transport (Glomset 1973). For this, cholesterol needs to be transferred from peripheral cells to the HDL particles and further to hepatocytes. Several mechanisms for cholesterol efflux and uptake might contribute: besides passive diffusion and the well-characterized cholesterol transfer via specific cell surface receptors, holo-HDL particle uptake and cholesterol exchange have been shown to take place.

Receptor-mediated HDL-derived cholesterol uptake was described by Acton et al. (1996), who demonstrated that Scavenger Receptor Class B, Type I (SR-BI) mediates selective uptake of HDL-derived cholesteryl ester without degradation of the particle. This process is a key mechanism in receptor-mediated delivery of HDL cholesteryl esters to liver and steroidogenic tissues (Krieger 1999), whereby only the cholesteryl esters of HDL particles are transferred to cells (Glass et al. 1983, 1985). In contrast to selective uptake, several alternative holo-HDL uptake pathways are discussed. First, an apoE-independent uptake and re-secretion pathway was described (Bierman et al. 1974; DeLamatre et al. 1990; Schmitz et al. 1985; Silver et al. 2001). More recently, SR-BI was identified as a receptor facilitating HDL uptake, which is followed by resecretion without degradation of HDL particles (Pagler et al. 2006; Rhode et al. 2004; Silver et al. 2001). Additionally, an SR-BI independent mechanism of HDL endocytosis, regulated by the nucleotide receptor $P2Y_{13}$, was described in hepatocytes (Jacquet et al. 2005; Martinez et al. 2003). Studies in rodent models of genetic obesity suggest that leptin participates in the regulation of plasma HDL levels in part by stimulating holo-HDL particle uptake by hepatocytes (Silver et al. 1999, 2000). Second, apoE-containing HDL is taken up by cells via B/E receptors and is subsequently degraded. Interestingly, apoE recycling has been reported to occur in hepatocytes and macrophages, where a part of the apoE associated with HDL escapes degradation (Hasty et al. 2005; Heeren et al. 2003). Third, the cubilin/amnionless-megalin receptor complex mediates endocytosis of both HDL and LDL in the proximal convoluted tubule of kidney and visceral yolk sac (Hammad et al.1999; Kozyraki et al. 1999; review: Moestrup and Nielsen 2005). Besides kidney, both receptors have been reported to play a role in the delivery of nutrients like cholesterol from the maternal to the fetal side of the placenta (Assemat et al. 2005;

Europe PMC Funders Author Manuscripts

Moestrup and Nielsen 2005). Although the renal clearance of apoA-I and the uptake of apoE-containing HDL via the LDL receptor family are well established, central facets of HDL particle uptake are still incompletely understood.

Recently, we have described that SR-BI over-expression results in increased holo-HDL particle uptake and resecretion in CHO cells (retroendocytosis), a pathway that has been demonstrated in the human hepatoma cell line HepG2 (Pagler et al. 2006). The liver is the central organ involved in lipoprotein metabolism. In particular, it promotes reverse cholesterol transport by mediating selective cholesteryl ester delivery from HDL, and also HDL catabolism, and HDL particle uptake and resecretion; nevertheless, detailed knowledge of holo-HDL particle uptake is missing.

To follow the uptake of HDL particles in HepG2 cells, we labeled the protein part of the lipoproteins for combined light and electron microscopic analyses. Different marker systems, horseradish peroxidase (HRP), colloidal gold, and fluorochromes were used to visualize the uptake and intracellular processing. The results obtained with the three markers, aside from specific advantages and disadvantages corresponded to each other. For a more detailed analysis of the light microscopical signals at higher resolution, we needed a marker system applicable for correlative light and electron microscopy. The dye Alexa^{568} proved most suitable to oxidize diaminobenzidine (DAB) during photooxidation-enabled correlative analyses at light microscopic and ultrastructural level.

During photooxidation, fluorescence signals are converted to electron dense precipitates visible in the electron microscope allowing to combine light and electron microscopic data (Maranto 1982). The underlying photooxidation reaction takes advantage of reactive oxygen species that form upon illumination of fluorescent dyes leading to oxidation of DAB in situ, which appears after osmium-staining as fine granular precipitate at the site of former fluorescent signals (Maranto 1982; Sosinsky et al. 2007). We established this photooxidation technique and localized different fluorochrome-tagged proteins and lipids electron microscopically (Meisslitzer-Ruppitsch et al. 2008). In this manuscript, we focus on the morphological characterization of holo-HDL particle uptake in HepG2 cells using combined and correlative microscopic methods to identify differently labeled HDL particles along their intracellular pathway. The concordant data identified multivesicular bodies (MVBs) as main endocytic compartments involved in holo-HDL particle passage.

Materials and methods

Cell culture

Cells were cultured according to standard procedures. HepG2 cells were maintained in minimal essential medium (MEM; Invitrogen, Eugene, OR, USA) supplemented with 10% fetal bovine serum (FBS; Invitrogen, Carlsbad, CA, USA), 1% non-essential amino acid solution (Sigma, St. Louis, MO, USA), 1 mmol/l sodium pyruvate (PAA, Austria) and penicillin/streptomycin (PAA). For photooxidation experiments cells were seeded on cover slips in 24-well plates at a density of 5×10^5 cells/well on day 0. For fluorescence microscopy cells were grown on Lab-TekII chamber slides (Nalge Nunc Int., IL, USA) at a density of 10^5 cells/well on day 0. On day 1, cells were washed twice with phosphate buffered saline (PBS) and refed with MEM containing 10% calf lipoprotein deficient serum (cLPDS). On day 2, cells were incubated with labeled HDL (HRP-HDL [25 and 100 μg/ml], gold-HDL [50 μg/ml], and HDL-Alexa^{568} [50 μg/ml]) diluted in MEM containing 2 mg/ml fatty acid-free bovine serum albumin (faf-BSA; PAA) at 37°C for 15 min to 3 h.

Lipoprotein preparation and labeling procedures

Plasma was collected from normolipidemic healthy volunteers, and HDL was recovered by serial ultracentrifugation at a density of 1.21 g/ml (Schumaker and Puppione 1986). The HDL fraction was routinely analyzed for its apolipoprotein content by SDS-gel electrophoresis. The apolipoprotein part of HDL was covalently labeled with Alexa^{568} (Molecular Probes, Eugene, OR, USA) including conjugation of HDL and dye at pH 8 and separation from unbound label by column chromatography using Sephadex G-25 (fine) resin (Sigma). Labeling ratios of 2:1 to 3:1 (dye:protein) were shown to give good results when used for DAB-photooxidation.

For preparation of HDL-gold particles, HDL was labeled with 20-nm colloidal gold particles as described by Handley et al. (1981). HDL-HRP conjugates were prepared utilizing the peroxidase labeling kit (Roche, Basel, Switzerland) according to the manufacturer's instruction.

Diaminobenzidine-photooxidation

DAB-photooxidation is used to convert fluorescent signals into electron-dense precipitates allowing their localization in the electron microscope. Cells were fixed with 4% formaldehyde and 0.5% glutaraldehyde in PBS at 4°C for 45 min. Thereafter, DAB photooxidation was performed as follows: cells were washed with buffer A (0.05 M Tris/HCl buffer pH 7.4) and pre-incubated with 1 mg/ml 3,3′-DAB (Sigma) in buffer A at room temperature for 30 min. DAB solutions were freshly prepared, filtered, and stored at 4°C. Illumination started in fresh DAB-solutions with a HBO 100-W high-pressure mercury vapor lamp utilizing a 40× objective (0.60 NA) and a TRITC filter set at 4°C; illumination time was 20 min. Afterwards, cells were washed with buffer A and postfixed in 1% osmium-ferrocyanide (1:1 mixture of 2% aqueous osmium tetroxide (OsO_4) and 3% potassium ferrocyanide; Merck, Darmstadt, Germany) for 15 min followed by 1% veronalacetate buffered OsO_4 at 4°C for 30 min.

HDL-horseradish peroxidase and HDL-gold

Cells were fixed with 2.5% glutaraldehyde in PBS, pH 7.4 for 30 min. HDL-HRP was visualized by demonstrating peroxidase activity via the classical DAB-oxidation reaction (Graham and Karnovsky 1966). After an overnight rinse in PBS, cells were postfixed in 1% OsO_4 for 4 h. For amplifying the electron density of the DAB-precipitate together with membrane contrast, samples were postfixed consecutively in OsO_4–ferrocyanide and OsO_4–veronalacetate (2 h) as indicated above. In the following, the samples were further processed for routine electron microscopy; after dehydration in a graded series of ethanol (50, 70, 90, 96, 100%), they were embedded in Epon (Serva, Heidelberg, Germany). 80–100-nm sections were cut with an UltraCut-UCT ultramicrotome (Leica Inc., Vienna, Austria), transferred to copper grids, and viewed either unstained or stained with uranyl acetate and lead citrate with a Zeiss EM900 transmission electron microscope equipped with a wide-angle Dual speed CCD camera (Albert Tröndle Dünzelbach, Moorenweis, Germany).

Immunofluorescence colocalizations

To further define the uptake pathway, colocalizations of internalized HDL-Alexa^{568} with antibodies against endogenous proteins, characteristic of compartments along the endocytic pathway ("organelle markers") were performed. The following primary rabbit antibodies were used: anti-early endosomal antigen I (EEAI; ABR, Rockford, IL, USA), anti-lysosomal integrated membrane protein II (LIMP-II; Novus, Littleton, CO, USA) and anti-*trans*-Golgi network 46-kDA protein (TGN-46; Sigma). Following HDL-Alexa^{568} incubation (15 min in the case of EEA1 colocalization and 3 h for LIMP-II and TGN-46 colocalizations), cells

were fixed with 3% formaldehyde in PBS for 30 min. Samples were then permeabilized with ice-cold methanol for 20 s and blocked with 2.5% BSA in PBS for 30 min, followed by incubation with primary antibodies diluted 1:250 in 1% BSA in PBS (buffer B) with 1% horse serum for 1 h and 3 rinses with buffer B containing 0.1% TWEEN-20. Next, cells were incubated with anti-rabbit Alexa^{488} (Molecular Probes) diluted 1:250 in buffer B with 1% horse serum. Subsequently cells were washed again with buffer B containing 0.2% TWEEN-20 and with PBS. Finally the samples were mounted with Fluoprep (Biomerieux, France) and visualized with a confocal microscope (LSM 510, Zeiss, Germany).

Semi-quantitative analysis of MVB number

The number of MVBs of individual sample sections was quantified in the TEM. Only cells exhibiting nuclei with a minimal diameter of 3 μm were evaluated. A minimum of 25 cells per sample were analyzed, and values were expressed as mean MVBs per cell. Polymorphic MVBs with few (<8), loosely packed vesicles and differently shaped appendices were pooled in one group classified as “class I”, whereas MVBs with more regular round profiles and tightly packed vesicles were classified as “class II”.

Electron tomography

The 200-nm sections of the Epon-embedded probes were cut in parallel to the plane of the cell monolayer and transferred to copper grids. Tomography was performed in a Tecnai 20 transmission electron microscope at 200 kV using a tilting stage (FEI Company, Eindhoven, The Netherlands) with a high tilt rotation tomography holder (Gatan Inc., Pleasanton, CA, USA) to orientate samples parallel to the tilting axis. Series with an angular range of −65 to +65° were recorded with a tilt increment of 1° using a Gatan slow-scan CCD camera (Gatan Inc.). Individual series were recorded automatically with the Xplore3D software (FEI Company). The images were aligned by using several itinerate cycles of cross-correlation of gray values, and the volume of the sections was reconstructed into serial slices using the software package Inspect 3D (FEI Company). Reconstruction into a 3D volume was performed by the weighted back projection method. The 3D-model was constructed by tracing the structures of interest on all virtual slices with colored membrane contours that are merged in the Z axis by Amira 4.1 software (Mercury Computer Systems, Merignac, Cedex, France). Virtual slices were approximately 1 nm thick.

Results

To characterize the cellular pathway of holo-HDL particle uptake and processing, HepG2 cells were incubated with differently labeled HDL particles, HDL-Alexa^{568}, HDL-HRP, and HDL-gold; all three conjugates, labeling the apolipoprotein moiety of HDL, revealed comparable labeling patterns. HDL-Alexa^{568} incubation resulted in a bright staining of large endocytic compartments found throughout the cytoplasm and accumulated in the perinuclear area (Fig. 1a). HDL-Alexa^{568} uptake was inhibited by the addition of a 50-fold excess of unlabeled HDL. After photooxidation using the Alexa^{568} signal to precipitate DAB, the stained endosomes were identified as MVBs (Fig. 1b, c). At all uptake times, HDL-positive and -negative MVBs were found side by side, which demonstrates not only the specificity of the method but also the complexity of the endocytic pathways. MVBs frequently showed tubular appendices and other protrusions of different shapes; the lumina of the MVBs were filled with reaction products, whereas the intraluminal vesicles (ILVs) constantly were devoid of staining (Fig. 1c; compare to 3e–h). Most but not all of the protrusions and appendices were reactive. Reaction product was also detected within coated pits and coated as well as smooth vesicles. To confirm the specificity of the correlative staining and the lack of artifacts generated by the photooxidation procedure, control experiments were done for every set of experiments. Control cultures grown without labeled HDL were processed

according to the DAB-photooxidation protocol (Fig. 1d); these probes were devoid of intracellular DAB precipitates, indicating that the HDL-Alexa^{568} driven staining is specific.

To verify and extend the findings obtained by DAB-photooxidation, we further used two classical labeling alternatives, enzymatic DAB-oxidation by HRP and colloidal gold as particulate marker. Comparable to the findings with DAB-photooxidation, HDL-HRP was localized preferentially in MVBs (Fig. 2a) and to a small extent in other endosomal compartments, such as small coated and non-coated vesicles; a slightly higher electron density of the HRP-DAB precipitate in small volume compartments as compared to photooxidation made their record more easy (see Fig. 5a). The staining of MVBs was in line with that obtained by DAB-photooxidation; MVBs showed labeled luminal contents but unstained ILVs. Homotypic fusions among MVBs, albeit rarely, were also observed (see Fig. 2a, inset). A portion of the MVBs always remained negative; the majority of lysosomes were devoid of staining.

For further substantiation, HepG2 cells were incubated with HDL-gold. The results corresponded to those achieved by the two other methods (Fig. 2b, c). Only the gold system enabled the clear cut differentiation of HDL-binding domains at the plasma membrane (Fig. 2d, e). Furthermore, HDL-gold was localized in endosomal compartments, with MVBs again exhibiting the highest HDL-gold-labeling (Fig. 2b, c). A comparable cellular distribution of the staining was found with the three different techniques. All three methods revealed a frequent localization of stained MVBs in close proximity to the *trans*-side of the Golgi-apparatus, but stacked Golgi cisternae and the TGN were negative (see Fig. 8).

The time-dependent progression of HDL uptake was systematically analyzed in time course experiments (Fig. 3). HepG2 cells were treated with HDL-Alexa^{568} for 15 min up to 3 h. Already 15 min after internalization, HDL-Alexa^{568} was seen in numerous endosomes (Fig. 3a); the plasma membrane exhibited hardly any staining. Fluorescent compartments increased in sizes, numbers and staining intensities over time (Fig. 3a–d). After DAB-photooxidation, stained MVBs were confirmed already at the early time points of HDL uptake (Fig. 3e). Consistent with the fluorescence data, HDL-positive MVBs increased in sizes and numbers, whereas HDL-negative MVBs decreased over time. Increase in size was paralleled by a change of the shapes, an increase in the number of ILVs and intensity of labeling. MVBs observed after short HDL-internalization times were irregular in shape, exhibited multiple and differently formed protrusions, including globular and tubular appendices, and loosely packed ILVs, whereas the profiles of the MVBs after longer times of HDL-uptake mostly were round, showed more uniform tubular appendices, and contained tightly packed ILVs. In general, at later HDL-internalization times, the MVBs appeared more compact than those at earlier time points (Fig. 3e–h). “Class II” MVBs (high number of ILVs, tightly packed, round profiles, and uniform tubular appendices; compare Fig. 3h) were enriched in the perinuclear area and the Golgi region, whereas irregular “class I” MVBs (low number of ILVs, loosely packed, irregular surfaces, and multiple differently formed protrusions; compare Fig. 3e, f) were found more dispersed in the cytoplasm. A possible influence of the marker system itself was tested by comparison of the time response of the intracellular progression of HDL-Alexa^{568} with those of HRP-HDL. Time course experiments with HDL-HRP led to very similar data in terms of uptake times and the intracellular compartments involved (data not shown).

Semi-quantitative analyses revealed that the number of HDL containing MVBs increased with time of uptake, reaching a plateau at about 60 min (Fig. 4). Based on structural criteria, “class I” MVBs and “class II” MVBs could be distinguished. The number of the “class II” MVBs (Fig. 3h) increased with time at the expense of the “class I” MVBs (Fig. 4). Noteworthy, MVBs were the main HDL-containing compartments at early internalization

times already, whereas a rather small number of other HDL containing early endosomal compartments (Fig. 5a) was identified, which might indicate a rapid transfer of HDL to MVBs. For confirmation, HepG2 cells were incubated with HDL-Alexa^{568} for 15–60 min and doublestained for detection of the early endosomal antigen I (EEAI). An overlap of HDL-Alexa^{568}- and EEAI-signals could be rarely demonstrated (Fig. 5b–d).

The structural organization of MVBs in the course of HDL uptake as a time-dependent process was studied three dimensionally. Differences between the two classes of MVBs concerned sizes and shapes, numbers of ILVs, and surface domains. For a closer examination of the latter, 200-nm thick sections were analyzed by electron tomography. Figure 6a–c shows three perspectives of a 3D model of a “class I” HDL-reactive MVB. The surface with the limiting membrane (green) is irregular and shows differently shaped protrusions and appendices, both with and without HDL-reaction products (red); HDL-reactions also are contained in the MVB’s lumen, whereas luminal vesicles (yellow) are devoid of staining.

The intracellular passage of HDL was examined with particular focus on a further transport to lysosomes and Golgi apparatus. Even after a long uptake time of 3 h, only a minor percentage of lysosomes contained stained HDL particles (Fig. 7a–c). For confirmation, HepG2 cells were incubated with HDL-Alexa^{568} for 3 h, fixed and double labeled for the lysosomal integrated membrane protein II (LIMP-II) as a lysosomal marker. LIMP-II positive compartments were accumulated in the perinuclear area and appeared as large ring-shaped structures (Fig. 7e); HDL-Alexa^{568} exhibited a different staining pattern (Fig. 7d) and showed only minor colocalization with LIMP-II reactions (Fig. 7f). This substantiates the ultrastructural findings that HDL only to a minor degree is transported to lysosomal compartments.

Stained MVBs were frequently localized in vicinity of the *trans*-side of the Golgi-apparatus (Figs. 8a, b, 9e), a finding already observed after short uptake times. However, with none of the markers, HDL was observed within the TGN-lumina or within stacked Golgi cisternae (Figs. 8a, b, 9e). Again, fluorescence double staining was used for confirmation. Cells incubated with HDL-Alexa^{568} were stained against TGN-46 kDa protein as TGN-marker (Fig. 8c–e). The TGN-46 fluorescence signal showed the known tubular cisternal network in the perinuclear area (Fig. 8d). HDL-stained compartments partially were found in proximity, but no colocalization was observed (Fig. 8e). On the other hand, electron microscopically, HDL-reactive appendices of MVBs were found to immerse into the Golgi region and to localize in close spatial relationship to membranes of the TGN (Fig. 8a).

As HDL is neither transported to lysosomes at large amounts nor found in the Golgi-apparatus, the question arises whether MVBs serve as a storage compartment for holo-HDL particles. Pulse chase experiments should figure out whether HDL-clearance from MVBs can be observed. HepG2 cells were treated with 50 μg/ml HDL-Alexa^{568} for 3 h, washed and kept in media containing the same amount of unlabeled HDL for up to 8 h. After 1 h of chase, the fluorescence intensity of stained vesicles was already considerably reduced (Fig. 9a, b). Further post-incubation with unlabeled HDL resulted in a time-dependent decrease of stained vesicles in number and size (Fig. 9c, d). Electron microscopy revealed that the number of HDL-positive MVBs declined essentially; only few HDL-positive compartments were apparent after 1 and 2 h of chase (Fig. 9f, g) and were hardly found after chase times longer than 4 h (Fig. 9h).

Finally, stained MVBs during pulse chase were analyzed semi-quantitatively as described above (Fig. 10). The numbers of stained MVBs were reduced to approximately one-third

within 1 h of chase; HDL-positive MVBs were hardly detectable after time-points longer than 4 h.

Discussion

In this study, we investigated the intracellular location of internalized holo-HDL particles in cells of the human hepatoma line HepG2 using fluorescence and electron microscopical methods combined with different labeling of the apolipoprotein moieties of HDL particles (HDL-Alexa^{568}, HDL-HRP and HDL-gold). While all three conjugates generally revealed comparable labeling patterns, differences were based on individual properties of the respective marker system. Membrane domains could be identified only with HDL-gold; on the other hand, the endocytic compartments visited by HDL, could be studied correlatively at light and electron microscopic levels with the photooxidation approach. With each of the marker systems, MVBs were identified as the central endocytic compartments taking part in the intracellular paths of internalized HDL. Following a peak of labeled MVBs about 1 h after onset of the HDL-pulse, HDL was cleared away from the MVBs again.

In order to enable correlative microscopy, optimal conditions for a photooxidation protocol had to be established in a first step. Among the tested HDL-conjugates, including the fluorochromes Alexa^{488} and Alexa^{568}, Cy2, and Cy3, Alexa^{568} proved most suitable to develop sufficient amounts of DAB-precipitates. Refinement of preparative steps around the photooxidation process proved to be necessary for the success of the reaction, the fine structural HDL-localization, as well as prevention of unspecific staining, fixation conditions, fluorochrome and DAB concentrations, and illumination conditions were adjusted (Meisslitzer-Ruppitsch et al. 2009). For the electron microscopic visualization of internalized HDL-Alexa^{568} particles an illumination time of 20 min is proved to be optimal. Unspecific precipitation developing at the plasma membrane already at these times argued for reduced illumination times; these opposed tendencies had to be considered in the protocol (Meisslitzer-Ruppitsch et al. 2009).

Ultrastructural localizations of fluorochrome-labeled lipoproteins by DAB photooxidation have been shown following the uptake of VLDL and βVLDL (Tabas et al. 1990) and of the insect lipoprotein lipophorin (Dantuma et al. 1998). In these studies, the neutral phospholipid DiI was used as fluorescent label. However, since DiI is not stably bound to the lipoprotein particle and diffusible and can easily cross the plasma membrane, it is not appropriate for our purpose to visualize holo-particle uptake. Both studies, working with DiI-lipoproteins report difficulties in the exact localization due to unspecific staining of small membrane compartments (Tabas et al. 1990); this could be avoided by blocking endogenous catalase activity by aminotriazole (Dantuma et al. 1998). In our experiments, blocking of endogenous radical sources was not necessary, since intracellular compartments were essentially negative for DAB-reaction product in control cells. Moreover, the specificity of the photooxidation signals was confirmed by the findings obtained with HRP- and gold-conjugated HDL. Uptake of fluorescently labeled HDL particles was correlatively shown by DAB-photooxidation. HDL was detected in endosomes and preferentially localized in MVBs increasing in sizes and numbers over time (Figs. 1, 3, 4). The fluorescence and electron microscopic data correlate well. Early endosomes were only infrequently HDL-positive in the TEM and, consistently, an overlap of the fluorescent signals for HDL- and EEAI-positive compartments could only rarely be found (Fig. 5). Staining of MVBs as early as 15 min after HDL-uptake indicates a rapid transfer process. This rapid internalization is in line with earlier studies, where HDL-uptake was followed by ultrasensitive fluorescence microscopy in CHO cells (Pagler et al. 2006; Rhode et al. 2004). We have previously provided evidence that in CHO cells SR-BI-over-expression results in a considerable augmentation of HDL uptake (Pagler et al. 2006). In HepG2 cells, however,

Europe PMC Funders Author Manuscripts

SR-BI siRNA knockdown leading to a 50% reduction of SR-BI protein levels did not result in significant reduction of cell association of iodinated HDL (own, unpublished data). Besides SR-BI, receptors for apoE—including the LDL-receptor, LRP1, and VLDL-receptor—are expressed in HepG2 cells (Röhrl et al. 2009). However, our HDL preparations do not contain apoE, and therefore those receptors are of limited importance for holo-HDL particle uptake (Pagler et al. 2006). These findings suggest the contribution of other receptors in this cell model; one candidate molecule expressed in HepG2 cells is the surface-expressed F1 subunit of the ATP-synthase, first described as an apolipoprotein A-1 receptor in hepatic HDL endocytosis (Martinez et al. 2003), which activates the nucleotide receptor $P2Y_{13}$ upon stimulation of extra-cellular ATP hydrolysis (Jacquet et al. 2005). Subsequent Rho- and ROCK-mediated downstream signaling results in clathrin-dependent endocytosis of HDL in HepG2 cells and primary human hepatocytes (Malaval et al. 2009).

Taken together, several lines of evidence revealed by immunolabeling, correlative microscopy and the use of various HDL-conjugates indicate that holo-HDL particles are rapidly taken up by HepG2 cells and enriched in MVBs. The change in the population of stained MVBs over time, from small, polymorphous, to compact, smooth surfaced compartments containing multiple, tightly packed vesicles (Fig. 3) suggests a maturation process. The differently shaped and labeled surface structures (Fig. 6), including globular protrusions and tubular appendices indicate dynamic transport of cargo into and out of MVBs (Woodman and Futter 2008).

Both confocal and electron microscopy showed that HDL is only to a minor degree transported to lysosomes (Fig. 7). Corresponding, Schmitz et al. (1985), using HDL-gold to analyze HDL uptake in cholesteryl ester-loaded macrophages, did not find fusion of HDL-positive compartments with lysosomes. This is in line with published own data showing that virtually no degradation of HDL can be measured in tissue culture (Stangl et al. 1998). This pathway essentially differs from the well-described uptake of LDL, which is finally transported to lysosomes for degradation (Brown and Goldstein 1986; Goldstein et al. 1985).

Pulse–chase experiments, performed to analyze the further passage of HDL-particles showed after an initial increase, with a plateau after about 1 h, a decrease of the number of stained MVBs after replacing labeled by unlabeled HDL during ongoing uptake. This indicates that MVBs constitute a temporary storage compartment (Figs. 9, 10). The HDL clearance during post-incubation is consistent with our earlier findings in CHO cells that internalized holo-HDL particles are re-secreted to the media as demonstrated by biochemical data and fluorescence microscopy. The time response of resecretion obtained by ^{125}I-HDL (Pagler et al. 2006) resembles our presented morphological data. As MVBs are the main HDL containing compartment, with only minor further HDL transfer to lysosomes, other pathways, such as exocytosis (de Gassart et al. 2004), transport to lipid droplets (Schmitz et al. 1985), and transport to the Golgi apparatus (Pavelka et al. 2008) have to be considered. Transport to the surface and release via small vesicular-tubular transport carriers, which possibly originate from globular and tubular MVB-surface domains, and export via secretion of exosomes (Harding et al. 1983; de Gassart et al. 2004) might play a role for holo-HDL re-secretion. Interestingly, proteomic analyses of exosomes derived from rat hepatocytes identified proteins involved in lipoprotein metabolism including apoA-V and apoE. However, the presence of apoA-I, apoA-II or apoC-II, the main HDL components, was not reported (Conde-Vancells et al. 2008).

HDL containing endocytic compartments were found in close association to lipid droplets in macrophages (Schmitz et al. 1985) as well as in polarized CaCo-2 cells (Klinger et al. 1997), probably mediating direct exchange of cholesterol between HDL and lipid droplets. Comparable associations of HDL-positive compartments and lipid droplets were observed

only rarely in our experiments indicating that direct cholesterol exchange from HDL to lipid droplets plays only a minor role in this model. In contrast, HDL-positive MVBs were frequently found within the Golgi region in close vicinity of the TGN (Figs. 8a, b, 9a), though *trans*-Golgi compartments and TGN themselves remained negative. Electron microscopic analysis of the cholesterol distribution in human lymphoblastoid cells showed MVBs and the TGN as those compartments of the endocytic pathway with the highest cholesterol content (Mobius et al. 2002, 2003). Thus, holo-HDL particles might be transported and temporarily stored in MVBs near the TGN for the exchange of HDL-derived cholesterol from MVBs directly toward the Golgi apparatus. The close Golgi apparatus associations of HDL-positive MVBs-appendices immersing into the *trans*-Golgi regions and residing in close spatial relationships to TGN membranes, as shown in Fig. 8a, underline this concept. Future work will focus on labeling of the lipid parts of HDL-particles to trace the delivery of lipids to the cell after holo-HDL particle uptake.

Acknowledgments

The authors would like to thank Mrs. Loredana Ionce, Mrs. Barbara Kornprat, Mrs. Beatrix Mallinger, and Mrs. Elfriede Scherzer for the excellent technical assistance, and thank Mr. Ulrich Kaindl for his valuable help with the artwork and the 3D model. This project is supported by the Austrian Science Fund (FWF) grant P20116.

References

Acton S, Rigotti A, Landschulz KT, Xu S, Hobbs HH, Krieger M. Identification of scavenger receptor SR-BI as a high density lipoprotein receptor. Science. 1996; 271:518–520. [PubMed: 8560269]

Assemat E, Vinot S, Gofflot F, Linsel-Nitschke P, Illien F, Chatelet F, Verroust P, Louvet-Vallee S, Rinninger F, Kozyraki R. Expression and role of cubilin in the internalization of nutrients during the peri-implantation development of the rodent embryo. Biol Reprod. 2005; 72:1079–1086. [PubMed: 15616221]

Bierman EL, Stein O, Stein Y. Lipoprotein uptake and metabolism by rat aortic smooth muscle cells in tissue culture. Circ Res. 1974; 35:136–150. [PubMed: 4366526]

Brown MS, Goldstein JL. A receptor-mediated pathway for cholesterol homeostasis. Science. 1986; 232:34–47. [PubMed: 3513311]

Conde-Vancells J, Rodriguez-Suarez E, Embade N, Gil D, Matthiesen R, Valle M, Elortza F, Lu SC, Mato JM, Falcon-Perez JM. Characterization and comprehensive proteome profiling of exosomes secreted by hepatocytes. J Proteome Res. 2008; 7:5157–5166. [PubMed: 19367702]

Dantuma NP, Pijnenburg MA, Diederen JH, Van der Horst DJ. Electron microscopic visualization of receptor-mediated endocytosis of Dil-labeled lipoproteins by diaminobenzidine photoconversion. J Histochem Cytochem. 1998; 46:1085–1089. [PubMed: 9705975]

De Gassart A, Geminard C, Hoekstra D, Vidal M. Exosome secretion: the art of reutilizing nonrecycled proteins? Traffic. 2004; 5:896–903. [PubMed: 15479454]

DeLamatre JG, Sarphie TG, Archibold RC, Hornick CA. Metabolism of apoE-free high density lipoproteins in rat hepatoma cells: evidence for a retroendocytic pathway. J Lipid Res. 1990; 31:191–202. [PubMed: 2324643]

Glass C, Pittman RC, Weinstein DB, Steinberg D. Dissociation of tissue uptake of cholesterol ester from that of apoprotein A-I of rat plasma high density lipoprotein: selective delivery of cholesterol ester to liver, adrenal, and gonad. Proc Natl Acad Sci USA. 1983; 80:5435–5439. [PubMed: 6412229]

Glass C, Pittman RC, Civen M, Steinberg D. Uptake of high-density lipoprotein-associated apoprotein A-I and cholesterol esters by 16 tissues of the rat in vivo and by adrenal cells and hepatocytes in vitro. J Biol Chem. 1985; 260:744–750. [PubMed: 3918032]

Glomset JA. The metabolic role of lecithin: cholesterol acyltransferase: perspectives from pathology. Adv Lipid Res. 1973; 11:1–65. [PubMed: 4354500]

Goldstein JL, Brown MS, Anderson RG, Russell DW, Schneider WJ. Receptor-mediated endocytosis: concepts emerging from the LDL receptor system. Annu Rev Cell Biol. 1985; 1:1–39. [PubMed: 2881559]

Graham RC, Karnovsky MJ. The early stages of absorption of injected horseradish peroxidase in the proximal tubules of mouse kidney: ultrastructural cytochemistry by a new technique. J Histochem Cytochem. 1966; 14:291–302. [PubMed: 5962951]

Hammad SM, Stefansson S, Twal WO, Drake CJ, Fleming P, Remaley A, Brewer HB Jr, Argraves WS. Cubilin, the endocytic receptor for intrinsic factor-vitamin B(12) complex, mediates high-density lipoprotein holoparticle endocytosis. Proc Natl Acad Sci USA. 1999; 96:10158–10163. [PubMed: 10468579]

Handley DA, Arbeeny CM, Witte LD, Chien S. Colloidal gold-low density lipoprotein conjugates as membrane receptor probes. Proc Natl Acad Sci USA. 1981; 78:368–371. [PubMed: 6264440]

Harding C, Heuser J, Stahl P. Receptor-mediated endocytosis of transferrin and recycling of the transferrin receptor in rat reticulocytes. The Journal of cell biology. 1983; 97:329–339. [PubMed: 6309857]

Hasty AH, Plummer MR, Weisgraber KH, Linton MF, Fazio S, Swift LL. The recycling of apolipoprotein E in macrophages: influence of HDL and apolipoprotein A-I. J Lipid Res. 2005; 46:1433–1439. [PubMed: 15805547]

Heeren J, Grewal T, Laatsch A, Rottke D, Rinninger F, Enrich C, Beisiegel U. Recycling of apoprotein E is associated with cholesterol efflux and high density lipoprotein internalization. J Biol Chem. 2003; 278:14370–14378. [PubMed: 12584196]

Jacquet S, Malaval C, Martinez LO, Sak K, Rolland C, Perez C, Nauze M, Champagne E, Terce F, Gachet C, Perret B, Collet X, Boeynaems JM, Barbaras R. The nucleotide receptor P2Y13 is a key regulator of hepatic high-density lipoprotein (HDL) endocytosis. Cell Mol Life Sci. 2005; 62:2508–2515. [PubMed: 16231090]

Klinger A, Reimann FM, Klinger MH, Stange EF. Clathrin-mediated endocytosis of high density lipoprotein3 in human intestinal Caco-2 cells. A post-embedding immunocytochemical study. Biochim Biophys Acta. 1997; 1345:65–70. [PubMed: 9084502]

Kozyraki R, Fyfe J, Kristiansen M, Gerdes C, Jacobsen C, Cui S, Christensen EI, Aminoff M, de la Chapelle A, Krahe R, Verroust PJ, Moestrup SK. The intrinsic factor-vitamin B12 receptor, cubilin, is a high-affinity apolipoprotein A-I receptor facilitating endocytosis of high-density lipoprotein. Nat Med. 1999; 5:656–661. [PubMed: 10371504]

Krieger M. Charting the fate of the “good cholesterol”: identification and characterization of the high-density lipoprotein receptor SR-BI. Annu Rev Biochem. 1999; 68:523–558. [PubMed: 10872459]

Malaval C, Laffargue M, Barbaras R, Rolland C, Peres C, Champagne E, Perret B, Terce F, Collet X, Martinez LO. RhoA/ROCK I signalling downstream of the P2Y13 ADP-receptor controls HDL endocytosis in human hepatocytes. Cell Signal. 2009; 21:120–127. [PubMed: 18948190]

Maranto AR. Neuronal mapping: a photooxidation reaction makes Lucifer yellow useful for electron microscopy. Science. 1982; 217:953–955. [PubMed: 7112109]

Martinez LO, Jacquet S, Esteve JP, Rolland C, Cabezon E, Champagne E, Pineau T, Georgeaud V, Walker JE, Terce F, Collet X, Perret B, Barbaras R. Ectopic beta-chain of ATP synthase is an apolipoprotein A-I receptor in hepatic HDL endocytosis. Nature. 2003; 421:75–79. [PubMed: 12511957]

Meisslitzer-Ruppitsch C, Vetterlein M, Stangl H, Maier S, Neumüller J, Freissmuth M, Pavelka M, Ellinger A. Electron microscopic visualization of fluorescent signals in cellular compartments and organelles by means of DAB-photoconversion. Histochem Cell Biol. 2008; 130:407–419. [PubMed: 18463889]

Meisslitzer-Ruppitsch C, Röhrl C, Neumüller J, Pavelka M, Ellinger A. Photooxidation technology for correlated light and electron microscopy. J Microscopy. 2009; 235:322–335. [PubMed: 19754726]

Mobius W, Ohno-Iwashita Y, van Donselaar EG, Oorschot VM, Shimada Y, Fujimoto T, Heijnen HF, Geuze HJ, Slot JW. Immunoelectron microscopic localization of cholesterol using biotinylated and non-cytolytic perfringolysin O. J Histochem Cytochem. 2002; 50:43–55. [PubMed: 11748293]

Mobius W, van Donselaar E, Ohno-Iwashita Y, Shimada Y, Heijnen HF, Slot JW, Geuze HJ. Recycling compartments and the internal vesicles of multivesicular bodies harbor most of the cholesterol found in the endocytic pathway. Traffic. 2003; 4:222–231. [PubMed: 12694561]

Moestrup SK, Nielsen LB. The role of the kidney in lipid metabolism. Curr Opin Lipidol. 2005; 16:301–306. [PubMed: 15891391]

Pagler TA, Rhode S, Neuhofer A, Laggner H, Strobl W, Hinterndorfer C, Volf I, Pavelka M, Eckhardt ER, van der Westhuyzen DR, Schutz GJ, Stangl H. SR-BI-mediated high density lipoprotein (HDL) endocytosis leads to HDL resecretion facilitating cholesterol efflux. J Biol Chem. 2006; 281:11193–11204. [PubMed: 16488891]

Pavelka M, Neumüller J, Ellinger A. Retrograde traffic in the biosynthetic-secretory route. Histochem Cell Biol. 2008; 129:277–288. [PubMed: 18270728]

Rhode S, Breuer A, Hesse J, Sonnleitner M, Pagler TA, Doringer M, Schutz GJ, Stangl H. Visualization of the uptake of individual HDL particles in living cells via the scavenger receptor class B type I. Cell Biochem Biophys. 2004; 41:343–356. [PubMed: 15509885]

Röhrl C, Fruhwürth S, Schreier SM, Lohninger A, Dolischka A, Hüttinger M, Zemann N, Hermann M, Strobl W, Stangl H. Scavenger receptor, Class B, Type I provides an alternative means for beta-VLDL uptake independent of the LDL receptor in tissue culture. Biochim Biophy Acta. 2009 doi: 10.1016/j.bbalip.2009.11.005.

Schmitz G, Robenek H, Lohmann U, Assmann G. Interaction of high density lipoproteins with cholesteryl ester-laden macrophages: biochemical and morphological characterization of cell surface receptor binding, endocytosis and resecretion of high density lipoproteins by macrophages. EMBO J. 1985; 4:613–622. [PubMed: 2988931]

Schumaker VN, Puppione DL. Sequential flotation ultracentrifugation. Methods Enzymol. 1986; 128:155–170. [PubMed: 3724500]

Silver DL, Jiang XC, Tall AR. Increased high density lipoprotein (HDL), defective hepatic catabolism of ApoA-I and ApoA-II, and decreased ApoA-I mRNA in ob/ob mice. Possible role of leptin in stimulation of HDL turnover. J Biol Chem. 1999; 274:4140–4146. [PubMed: 9933608]

Silver DL, Wang N, Tall AR. Defective HDL particle uptake in ob/ob hepatocytes causes decreased recycling, degradation, and selective lipid uptake. J Clin Invest. 2000; 105:151–159. [PubMed: 10642593]

Silver DL, Wang N, Xiao X, Tall AR. High density lipoprotein (HDL) particle uptake mediated by scavenger receptor class B type 1 results in selective sorting of HDL cholesterol from protein and polarized cholesterol secretion. J Biol Chem. 2001; 276:25287–25293. [PubMed: 11301333]

Sosinsky GE, Giepmans BN, Deerinck TJ, Gaietta GM, Ellisman MH. Markers for correlated light and electron microscopy. Methods Cell Biol. 2007; 79:575–591. [PubMed: 17327175]

Stangl H, Cao G, Wyne KL, Hobbs HH. Scavenger receptor, class B, type I-dependent stimulation of cholesterol esterification by high density lipoproteins, low density lipoproteins, and nonlipoprotein cholesterol. J Biol Chem. 1998; 273:31002–31008. [PubMed: 9812997]

Tabas I, Lim S, Xu XX, Maxfield FR. Endocytosed beta-VLDL and LDL are delivered to different intracellular vesicles in mouse peritoneal macrophages. J Cell Biol. 1990; 111:929–940. [PubMed: 2391369]

Woodman PG, Futter CE. Multivesicular bodies: co-ordinated progression to maturity. Curr Opin Cell Biol. 2008; 20:408–414. [PubMed: 18502633]

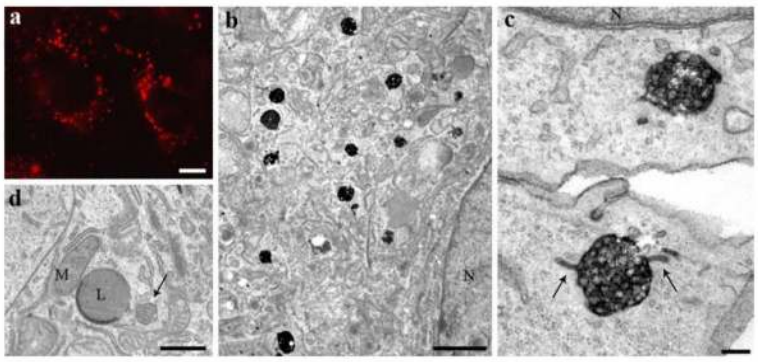

Fig. 1.

Correlative fluorescence and electron microscopic localization of HDL. HepG2 cells were incubated with 50 μg/ml HDL-Alexa^{568} for 3 h. In the fluorescence microscope, HDL is found in bright, large endocytic compartments enriched in the perinuclear area (**a**). After DAB-photooxidation, numerous MVBs are positive for internalized HDL (**b**). Their matrix and the intraluminal vesicle membrane are heavily stained (**c**). Tubular appendices are frequently positive (*arrows*). Control cells incubated without labeled HDL were equally processed according to the photooxidation protocol. Cellular compartments including MVBs (*arrow*), mitochondria (*M*), and lysosomes (*L*) are devoid of DAB precipitate (**d**). Primary magnifications: 1,000× (**a**), 8,000x (**b**), 90,000x (**c**), 10,000x (**d**). *Bars* 5 μm (**a**), 1 μm (**b**), 100 nm (**c**), 500 nm (**d**); *N* nucleus

Europe PMC Funders Author Manuscripts

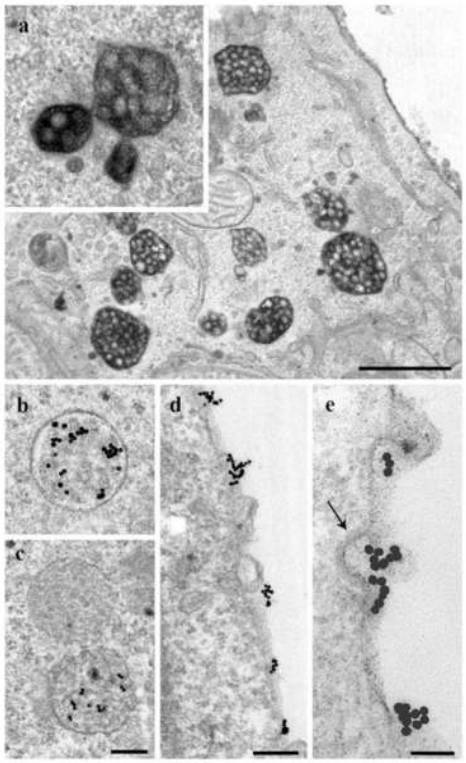

Fig. 2.

Localization of HDL-HRP and HDL-gold. After 3-h internalization, HDL-HRP marks a multitude of MVBs (**a**). Homotypic fusions of stained MVBs different in sizes and shapes are present (*inset*). Incubation with HDL-gold for 3 h shows a comparable staining of endosomal compartments and enrichment in MVBs (**b, c**). HDL-gold positive and negative MVBs may be found side by side (**c**). With the HDL-gold system discrete PM domains (**d, e**) and binding to clathrin-coated pits are discerned (*arrow*; **e**). Primary magnifications: 17,000x (**a**), 28,000x (**b, c**), 40,000x (**d**), 80,000x (**e**). *Bars* 1 μm (**a**), 250 nm (**b, c**), 200 nm (**d**), 100 nm (**e**)

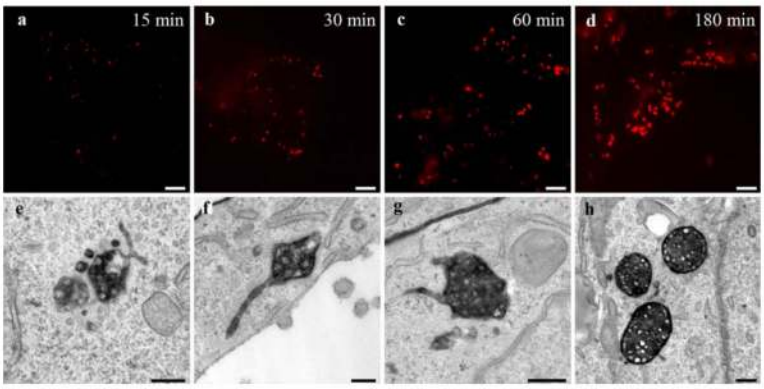

Fig. 3.

Time course of HDL internalization. Correlative HDL-Alexa^{568} localization after the indicated time points from 15 to 180 min shows in the fluorescence microscope a time-dependent increase in size and number of intracellular endocytic compartments (**a**–**d**). Electron microscopy after DAB-photooxidation reveals that HDL-positive compartments are preferentially MVBs even after the shortest time point of incubation (**e**–**h**). The shapes of the MVBs change, their surface becomes smoother, their sizes as well as the numbers of internal vesicles increase over time, MVBs become more compact, whereas the tubular appendices decrease in numbers and lengths and become more uniform. Primary magnifications: 1,000x (**a**–**d**), 75,000x (**e**), 55,000x (**f**), 85,000x (**g**), 45,000x (**h**). *Bars* 5 μm (**a**–**d**), 100 nm (**e**–**h**)

Europe PMC Funders Author Manuscripts

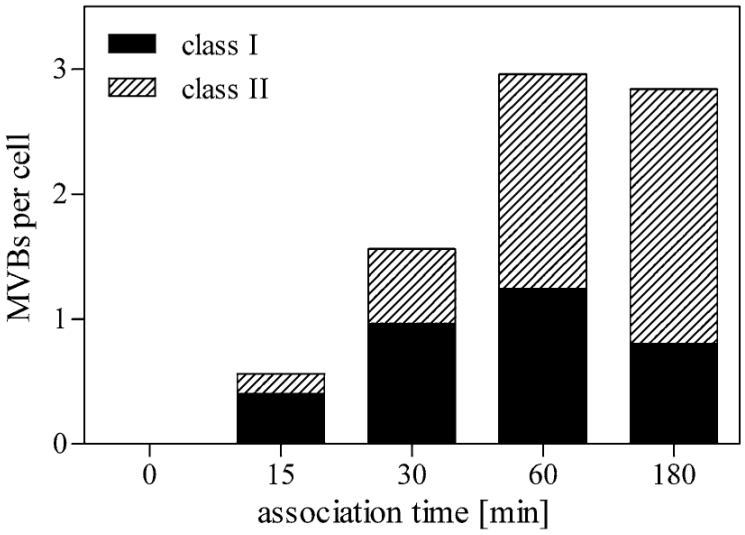

Fig. 4.

Semi-quantitative analysis of HDL-positive MVBs during a 3-h time course. The number of stained MVBs after HDL internalization and DAB-photooxidation was counted and expressed as mean number per cell. Bodies with few loosely packed internal vesicles (<8) and differently shaped appendices were classified as “class I” MVBs; organelles with round profiles and many tightly packed vesicles were classified as “class II” MVBs. Stained MVBs increase over time reaching a plateau after 60 min. Although the number of stained MVBs remains constant within the time period from 60 to 180 min, “class II” MVBs increase over time at the expense of “class I” MVBs

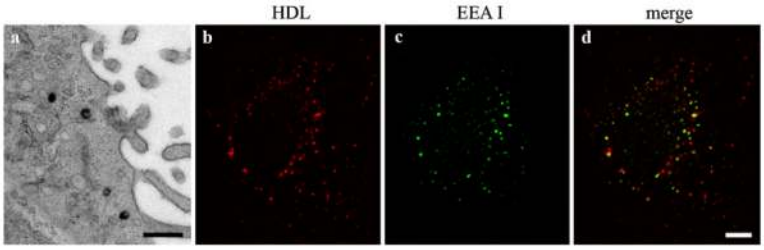

Fig. 5.

Localization of HDL in early endosomal compartments. One hour after incubation of HepG2 cells with 50 μg/ml HDL-Alexa^{568} few early endocytic compartments were stained after photooxidation (**a**). EEAI showed a fine punctated fluorescence (**c**). The cellular distribution of HDL-Alexa^{568} (**b**) and early endosomal compartments (**c**) looks similar; however, colocalization (**d**, *yellow spots*) is limited. Primary magnifications: 18,000× (**a**), 1,000× (**b**–**d**). *Bar* 500 nm (**a**), 5 μm (**b**–**d**)

Europe PMC Funders Author Manuscripts

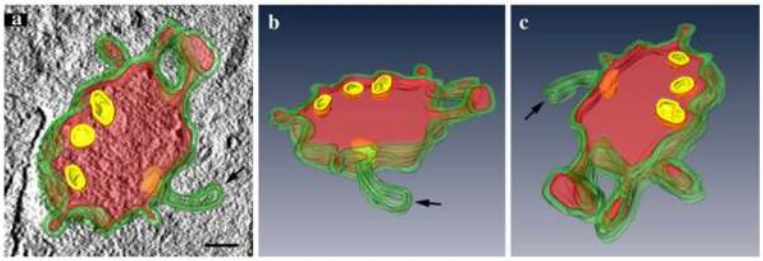

Fig. 6.

Three-dimensional reconstruction of a HDL-positive MVB. HDL-positive MVBs after 3 h of HDL internalization were analyzed by electron tomography. The 3D reconstruction of a 200-nm section demonstrates differently shaped domains of the MVB's limiting membrane, including elongated and globular protrusions and a tubular appendix (**a**–**c**). Reaction products are colored in *red*. The three perspectives of the model, in **a** shown together with a tomographic slice, give insight into HDL-positive and negative (*arrow*) appendices; the intraluminal vesicles (*yellow*; selected ILVs were chosen for reconstruction) are devoid of reaction products (**a**–**c**). Primary magnification: 60,000×. *Bar* 100 nm

Europe PMC Funders Author Manuscripts

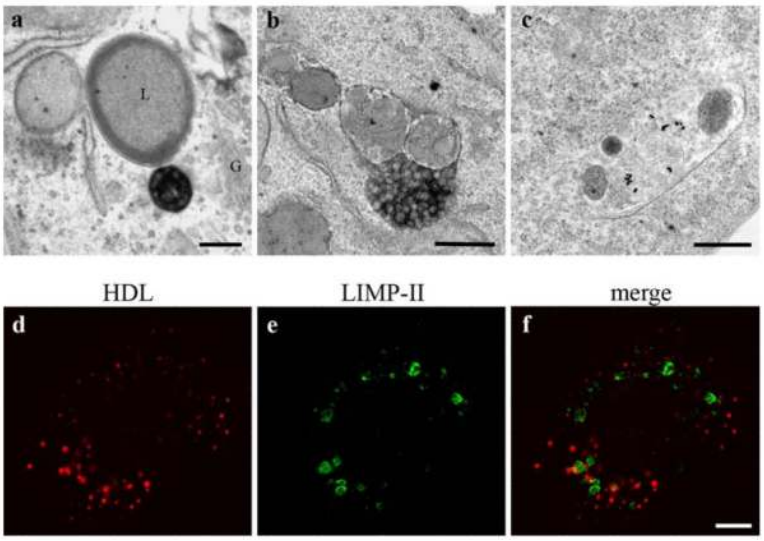

Fig. 7.

HDL is rarely found in lysosomes. Three hours after uptake of HDL-Alexa^{568} and DAB-photooxidation, a HDL-positive MVB is localized in the Golgi region (*G*) close to a lysosome (*L*); both, the Golgi apparatus and the lysosome are devoid of reactions (**a**). The very rarely observed uptake of internalized HDL in a lysosome is shown with HDL-HRP in **b**, and with HDL-gold in **c**. Poor colocalization between HDL-Alexa^{568} and the lysosomal marker LIMP-II (**d**–**f**) confirm these findings. Primary magnifications: 28,000× (**a**), 40,000× (**b, c**), 1,000× (**d**–**f**). *Bar* 250 nm (**a**–**c**), 5 μm (**d**–**f**)

Europe PMC Funders Author Manuscripts

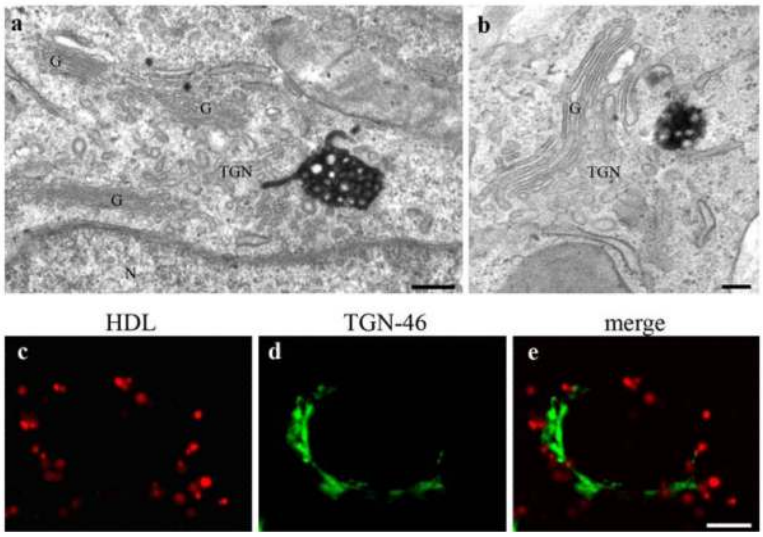

Fig. 8.

HDL-positive MVBs are localized in the Golgi region. Photooxidation and TEM analyses after 3 h of HDL incubation reveals that MVBs are frequently found close to the Golgi stacks (**a, b**). Stacked Golgi cisternae (*G*) as well as the *trans*-Golgi network (TGN) are devoid of staining (**a, b**); in **a**, a HDL-positive appendix of the MVB immerses into the Golgi region and is localized in close spatial relationship to membranes of the TGN. TGN-46 immunolocalization shows an extensive stained tubulo-cisternal network on one side of the nucleus (**d**). HDL-Alexa^{568} on the contrary stains spotty vesicles surrounding the nucleus (**c**), but no colocalization is observed (**e**). Primary magnifications: 75,000× (**a**), 50,000× (**b**), 1,000× (**c**–**e**). *Bar* 100 nm (**a, b**); 5 μm (**c**–**e**); *G* Golgi apparatus; *N* nucleus

Europe PMC Funders Author Manuscripts

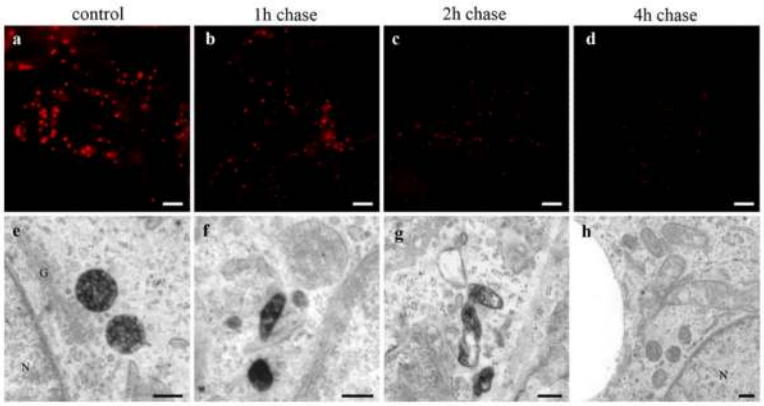

Fig. 9.

Clearance of HDL from MVBs. HepG2 cells were incubated with 50 μg/ml HDL-Alexa^{568} for 3 h (control) and further incubated with media containing 50 μg/ml unlabeled HDL for the indicated time points. Cells were imaged by fluorescence microscopy (**a**–**d**) or further processed for DAB photooxidation and TEM (**e**–**h**). Numbers, sizes, and staining intensities of HDL-Alexa^{568} positive compartments decrease time dependently (**a**–**d**). Concomitantly in the electron microscope (**e**–**h**), MVBs are reduced considerably in favor of smaller polymorphous HDL-reactive compartments (**f, g**). After 4-h post-incubation, nearly all MVBs are negative for HDL staining (**h**). Primary magnifications: 1,000× (**a**-–**d**), 70,000x (**e, f**), 55,000x (**g**), 35,000x (**h**). *Bar* 5 μm (**a**–**d**), 200 nm (**e**), 100 nm (**f**–**h**); *N* nucleus; *G* Golgi apparatus

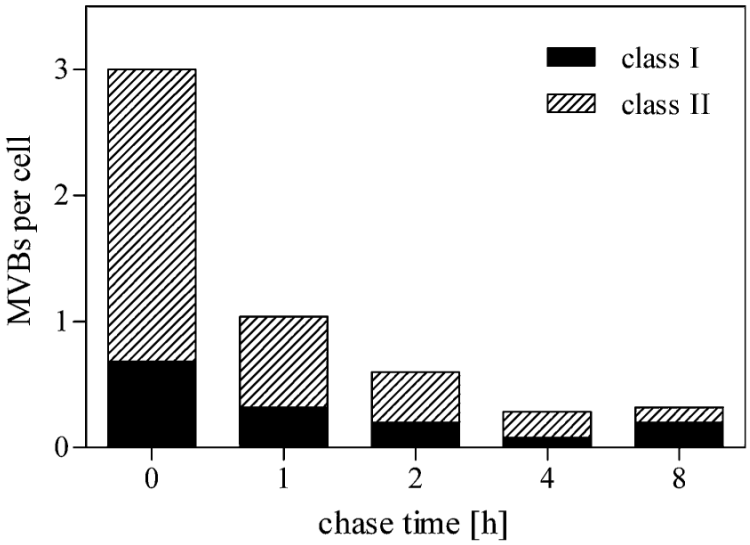

Fig. 10.

Semi-quantitative analysis of MVBs during pulse chase. Pulse chase experiments were performed as described in Fig. 9 and HDL-positive MVBs were analyzed semi-quantitatively as described. The numbers of “class II” as well as “class I” MVBs decrease substantially after a 1-h chase period. After 4 h, HDL-positive MVBs are hardly detectable